

Asymmetric rotations and dimerization driven by normal to modulated phase transition in 4-biphenylcarboxy coupled L-phenylalaninate

SOMNATH DEY,^{a,b*} SUPRIYA SASMAL,^a SAIKAT MONDAL,^a SANTOSH KUMAR,^a
 RITUPARNO CHOWDHURY,^a DEBASHRITA SARKAR,^a C. MALLA REDDY,^a
 LARS PETERS,^b GEORG ROTH^b AND DEBASISH HALDAR^a

^a*Department of Chemical Sciences, Indian Institute of Science Education and Research (IISER) Kolkata, Mohanpur 741246 India, and* ^b*Institute of Crystallography, RWTH Aachen University, Jägerstraße 17-19, 52066 Aachen Germany. E-mail: dey@ifk.rwth-aachen.de*

Abstract

Amongst the derivatives of 4-biphenylcarboxylic acid and amino acid esters, the crystal structure of 4-biphenylcarboxy-(L)-phenylalaninate is unusual owing to its monoclinic symmetry within a pseudo-orthorhombic lattice. The distortion is described by disparate rotational property around the chiral centers ($\varphi_{\text{chiral}} \simeq -129$ degrees and 58 degrees) of the two molecules in the asymmetric unit. Each of these molecules comprise of planar biphenyl moieties ($\varphi_{\text{biphenyl}} = 0$ degrees). Using temperature dependent single crystal X-ray diffraction experiments we show that the compound undergoes a phase transition below $T \sim 124$ K that is characterized by a commensurate modulation wave vector, $\mathbf{q} = \delta(101)$, $\delta = \frac{1}{2}$. The (3+1) dimensional modulated structure at

$T = 100$ K suggests that the phase transition drives the biphenyl moieties towards non coplanar conformations with significant variation of internal torsion ($\varphi_{\text{biphenyl}}^{\text{max}} \leq 20$ degrees). These intramolecular rotations lead to dimerization of the molecular stacks that are described predominantly by intermolecular tilts and small variations in intermolecular distances. Atypical of modulated structures and superstructures of biphenyl and other polyphenyls, the rotations of individual molecules are asymmetric ($\Delta\varphi_{\text{biphenyl}} \approx 5$ degrees) while $\varphi_{\text{biphenyl}}$ of one independent molecule is two to four times larger than the other. Crystal-chemical analysis and phase relations in superspace suggest multiple competing factors involving intramolecular steric factors, intermolecular H–C···C–H contacts and weak C–H···O hydrogen bonds that govern the distinctively unequal torsional property of the molecules.

1. Introduction

Molecular biphenyl has been investigated extensively for its stability and conformation in different thermodynamic states. At ambient conditions, the differences in the conjugation states of the π -electrons are governed primarily by the twist about the central C–C single bond in the order: 40 deg - 45 deg in gas phase, 20 deg - 25 deg in solution and 0 deg (mutually coplanar) in the solid state in centrosymmetric monoclinic space group $P2_1/a$ (Bastiansen, 1949; Suzuki, 1959; Trotter, 1961; Hargreaves & Rizvi, 1962). The planar conformation due to constraints from intermolecular interactions is energetically unfavourable and steric hindrance between the ortho hydrogen atoms is compensated for by out of plane dynamic disorder and in plane displacements of those hydrogens away from each other (Hargreaves & Rizvi, 1962; Casalone *et al.*, 1968; Charbonneau & Delugeard, 1976; Charbonneau & Delugeard, 1977; Busing, 1983; Lenstra *et al.*, 1994) A recent study has also suggested the role of intramolecular exchange energy between single bonded carbon atoms in stabilizing

the planar conformation (Popelier *et al.*, 2019). Absorption and fluorescence studies showed additional bands in their spectra at low temperatures (T) (Hochstrasser *et al.*, 1973; Wakayama, 1981). T -dependent Raman spectroscopy and Brillouin scattering experiments have suggested two phase transitions at $T_{c1} = 42$ K and $T_{c2} = 17$ K respectively (Friedman *et al.*, 1974; Bree & Edelson, 1977; Bree & Edelson, 1978; Ecolivet & Sanquer, 1983). The phase transition at T_{c1} is continuous and governed by a soft mode associated with the torsion about the central C–C single bond followed by discontinuous changes at T_{c2} . Inelastic neutron scattering experiments on its deuterated form confirmed the phase transitions with appearance of additional satellite reflections (Cailleau *et al.*, 1978). The modulation wave vector (\mathbf{q}) was determined to be $\mathbf{q}_I = \delta_a \mathbf{a}^* + \frac{1}{2}(1 - \delta_b) \mathbf{b}^*$ and $\mathbf{q}_{II} = \frac{1}{2}(1 - \delta_b) \mathbf{b}^*$ at the intermediate and low temperature phases respectively and were found to vary with temperature, suggesting an incommensurate nature of the modulation (Cailleau *et al.*, 1978). The modulated structure of the low temperature phase II was described within an acentric superspace group symmetry $Pa(0\sigma_20)0$ (de Wolff, 1974; Stokes *et al.*, 2011; van Smaalen *et al.*, 2013) and found to be essentially associated with small modulation of translation and rotation (ω) normal to the mean molecular plane, and a significant torsion (φ) between the phenyl rings (Baudour & Sanquer, 1983; Petricek *et al.*, 1985; Pinheiro & Abakumov, 2015; Schoenleber, 2011). Theoretical studies have suggested that competition between intramolecular and intermolecular forces drives the phase transition towards the incommensurately modulated states (Ishibashi, 1981; Benkert *et al.*, 1987; Benkert & Heine, 1987; Parlinski *et al.*, 1989).

The fundamental property of flexibility in conformations have made biphenyl an excellent candidate to tune in multifaceted properties in materials. Torsion between the rings has been demonstrated to regulate conductivity of single molecule biphenyl-dithiol junctions (Vonlanthen *et al.*, 2009; Mishchenko *et al.*, 2010; Buerkle *et al.*,

2012; Jeong *et al.*, 2020), tune in thermopower as function of twist angle (Buerkle *et al.*, 2012), degeneracy of energy states on substrates (Cranney *et al.*, 2007) and theoretically suggest wide band gap semiconducting properties of its derivatives (Khatua *et al.*, 2020). On the other hand, biphenyl derivatives have also been reported to influence and increase the efficiency of photophysical properties (Oniwa *et al.*, 2013; Wei *et al.*, 2016). Planar biphenyl molecule in solid state favours maximum intramolecular conjugation of π electrons as well as increases the probability of interactions between delocalized electrons that could aid in optimal stacking of molecules. Coupling reaction mechanism (Seechurn *et al.*, 2012) was successfully employed to synthesize 4-biphenylcarboxy protected amino acid esters of L-serine, L-tyrosine, L-alanine, L-leucine and L-phenylalanine (Sasmal *et al.*, 2019b; Sasmal *et al.*, 2019a). In solid state, the compounds crystallize either in acentric orthorhombic space group symmetry $P2_12_12_1$ or the monoclinic subgroup $P2_1$ (Sasmal *et al.*, 2019b; Sasmal *et al.*, 2019a). Crystal packing in these systems is determined by $\pi\cdots\pi$ stacking between the biphenyl fragments and linear strong hydrogen bonds between the amino acid ester moieties.

We presumed that the biphenyl moieties in these chemically coupled systems could influence the bioactive amino acid esters and *vice-versa* with respect to evolution or suppression of translational and rotational degrees of freedom in their crystal structures at some thermodynamic condition. Reanalyzing all their crystal structures, the system of 4-biphenylcarboxy-(L)-phenylalaninate attracted our attention because the structure appeared to be similar to the L-tyrosine analogue albeit the monoclinic distortion (Table 1, (Sasmal *et al.*, 2019a)) and two crystallographically independent formula units [$Z' = 2$ (Steed & Steed, 2015), Fig. 4(a)] in the crystal structure of the former. The torsion about the chiral center is significantly different for the independent molecules while the rest of the rotations are similar [Fig. 4(a), (Sasmal *et al.*, 2019a)]. Each of these molecules consist of coplanar biphenyl moieties which are stacked along

a and **b** respectively while the amide groups are connected by intermolecular N–H···O hydrogen bonds [Fig. 4(b),(Sasmal *et al.*, 2019a)].

In the present study, T -dependent phase transition of 4-biphenylcarboxy-(L)-phenylalaninate has been investigated using single crystal X-ray diffraction experiments. The low temperature phase II is found to be a $2a \times b \times 2c$ superstructure of the high temperature (phase I) structure. The superstructure is described within the $(3 + 1)D$ super-space approach as a commensurately modulated structure (de Wolff, 1974; Janner & Janssen, 1977; Wagner & Schoenleber, 2009; van Smaalen, 2012; Janssen *et al.*, 2018). Structural properties of the phase I and the modulated structure have been tabulated and compiled within t -plots (t = phase of the modulation). The origin and stability of phase II is discussed in terms of intra- and intermolecular HC···CH contacts and intermolecular hydrogen bonds and plausible mechanism of the phase transition is suggested.

2. Experimental

2.1. Temperature dependent single crystal X-ray diffraction

Single crystals of the compound used in this study were obtained from those reported by (Sasmal *et al.*, 2019a). The crystals were protected in oil under mild refrigeration. Single crystal X-ray diffraction (SCXRD) experiments were performed on a Agilent SuperNova, Eos diffractometer employing $\text{CuK}\alpha$ radiation. Temperature of the crystal was maintained by a open flow nitrogen cryostat from Oxford Cryosystems. During cooling, visual inspection of diffraction images revealed weaker reflections in addition to strong reflections at low temperatures. Diffraction images collected at $T = 150$ K, 140 K and 130 K to 114 K in steps of $\Delta T = 2$ K showed that the weaker diffuse features appear at $T = 124$ K that condense into satellite reflections at $T = 122$ K (Table 1, Fig. S1 in supporting information). The transition temperature is sig-

nificantly higher than that of molecular biphenyl ($T_{c,\text{biphenyl}} = 42$ K). On the other hand, related polyphenyls *p*-terphenyl and *p*-quarterphenyl undergo phase transition towards superstructure phases at much higher critical temperatures ($T_{c,\text{terphenyl}} \approx 190$ K (Yamamura *et al.*, 1998), $T_{c,\text{quarterphenyl}} \approx 233$ K (Saito *et al.*, 1985)). Complete diffraction data were collected at $T = 160$ K and $T = 100$ K respectively.

Determination of lattice parameters and data reductions were performed using the software suite CRYALISPRO (Cry, 2019) (Table 1, Table S1 in supporting information). Satellite reflections of first order ($m = 1$) observed below T_c could be indexed with modulation wave-vector $\mathbf{q} = (\sigma_1, 0, \sigma_3)$, $\sigma_1 = \sigma_3 \simeq \frac{1}{2}$ with respect to the basic monoclinic lattice. Here, the $\mathbf{q} = \frac{1}{2}(101)$ is perpendicular to the \mathbf{b} axis consistent with monoclinic symmetry while in molecular biphenyl \mathbf{q}_I violates monoclinic symmetry and \mathbf{q}_I is parallel to \mathbf{b} (Cailleau *et al.*, 1978). Using the plugin program NADA (Schoenleber *et al.*, 2001) in CRYALISPRO, deviation of the σ 's as function of T from a rational value of 0.5 were found to be within their e.s.ds (Table 1), indicating a commensurate nature of the modulation. Reflections at $T = 100$ K were indexed by four integers ($hklm$) using a basic monoclinic *b*-unique lattice (Table 1, Table S1 in supporting information) and modulation wave vector, $\mathbf{q} = (\frac{1}{2}, 0, \frac{1}{2})$ and data integration was performed. Empirical absorption correction was performed using ABSPACK program embedded in CRYALISPRO. The monoclinic lattice as well as the reflection conditions suggest the superspace group $P2_1(\sigma_1 0 \sigma_3)0$ with $\sigma_1 = \sigma_3 = \frac{1}{2}$ (Stokes *et al.*, 2011; van Smaalen *et al.*, 2013).

2.1.1. Structure refinement of the modulated structure The crystal structure of the room temperature phase (phase I hereon) was redetermined at $T = 160$ K using SUPERFLIP (Palatinus & Chapuis, 2007) and refined using JANA2006 (Petricek *et al.*, 2014) and JANA2020 (Petricek *et al.*, 2022). Atoms were renamed with suffixes ‘a’

and ‘b’ for the two independent molecules ‘A’ and ‘B’ [Fig. 4(a)]. Anisotropic atomic displacement parameters (ADPs) of all non-hydrogens atoms were refined. Hydrogen atoms (H) were added to carbon and nitrogen atoms using riding model in ideal chemical geometry with constraints for isotropic ADPs [$U_{iso}(\text{H}) = 1.2U_{eq}(\text{N})$, $U_{iso}(\text{H}) = 1.2U_{eq}(\text{C}_{\text{aromatic}})$ and $U_{iso}(\text{H}) = 1.5U_{eq}(\text{C}_{sp3})$]. Since β is close to 90 deg, the integrated data was tested for twinning employing twofold rotation parallel **a** as twin law. This twin law is a true symmetry element in case of a hypothetical orthorhombic lattice with point group symmetry 222 (Petricek *et al.*, 2016; Nespolo, 2019). The fit of the structure model improved (compare $R_F^{obs} = 0.0463$ to 0.0408) and volume of the second component refined to $\sim 2\%$ (Table S2 in supporting information). Finally, positions of the H atoms of NH groups and parameter corresponding to isotropic extinction correction was refined that further improved R_F^{obs} values (= 0.0393, Table S2 in supporting information). The crystal structure reproduced the values for intramolecular rotations reported those for the structure at $T = 200$ K [$\varphi_{\text{chiral}} = \varphi_1$ (hereon) and ψ in Fig. 4(a)]. In addition, we also observe that the coplanar biphenyl rings are significantly rotated with respect to the amide groups [at $T = 200$ K: $\varphi_2 = 32.8$ deg and 31.2 deg (Sasmal *et al.*, 2019a), at $T = 160$ K in Fig. 4(a)] which also remains invariant as function of temperature.

The modulated structure of phase II at $T = 100$ K was refined using JANA2006 and JANA2020. Fractional co-ordinates of all non-hydrogen atoms from the crystal structure at $T = 160$ K were used as starting model and the average structure was refined against main reflections. In successive steps, an incommensurate (IC) model described by one harmonic wave for displacive modulation describing the atomic modulation functions (AMFs) and basic parameters for anisotropic ADPs for all atoms was refined against main and satellite reflections that resulted in good fit to the diffraction pattern ($R_F^{obs} = 0.0425$). However, ADPs of four non-hydrogen atoms were found

to be non-positive definite. Since the components of \mathbf{q} , σ_1 and σ_3 are rational, three commensurately modulated structures were pursued by fixing the initial phase of the modulation to values, $t_0 = 0$, $\frac{1}{4}$ and $\frac{1}{8}$ respectively. While the former two t_0 values describe monoclinic $B2_1$ space group symmetry for the equivalent 3D $2a \times b \times 2c$ superstructure, the third corresponds to triclinic $B1$ symmetry. The commensurately modulated structure (C) model corresponding to $t_0 = \frac{1}{4}$ resulted in the best fit to the diffraction data ($R_F^{obs} = 0.0426$) including ADPs of all atoms positive definite. As the atomic modulation functions (AMFs) have sinusoidal character, the residual values are similar to the IC model (Fig. 4, Fig. S2-S4 and Table S2 in supporting information) However, the C model at $t_0 = \frac{1}{4}$ is described with either cosine or sine waves for the AMFs (equal to number of refinable fractional coordinates in the equivalent superstructure) reducing significantly the number of refinable parameters as compared to the IC model (compare $N_C = 649$ to $N_{IC} = 811$, further tests in supporting information). The final C model was further improved by refining the parameter corresponding to isotropic extinction correction and AMFs and positions of hydrogen atoms of NH groups ($R_F^{obs} = 0.0419$, Table S2 in supporting information).

3. Results and discussion

3.1. Structural phase transition and unequal distortion of molecules

In the present case, the monoclinic symmetry is retained below T_c unlike monoclinic to triclinic distortion at disorder–order phase transition of *p*-terphenyl (Rice *et al.*, 2013) and *p*-quarterphenyl (Baudour *et al.*, 1978). In the final commensurately modulated structure model with $t_0 = \frac{1}{4}$, sections corresponding to $t = \frac{1}{4}$ and $\frac{3}{4}$ (Fig. 4, Fig. S5 in supporting information) are physically relevant that corresponds to atomic positions in the equivalent twofold superstructure in 3D (Fig. 4, Fig. S6 in supporting information). Crystal structures of phase I and phase II have group-subgroup rela-

tions and the doubling of the a and c axes describes the additional B -centering of the superstructure in II. The superstructure derived using JANA2006 comprises of four molecules in the asymmetric unit ($Z' = 4$); two each corresponding to molecule ‘A’ and ‘B’ of phase I (Fig. 4). The covalent bond distances are similar for the independent set of molecules and are practically unaffected by modulation (Table S6 in supporting information). In the present study, discussion is based on the modulated structure in order to establish unique relations between phase I and II respectively (Rekis *et al.*, 2021; Ramakrishnan *et al.*, 2019; Dey *et al.*, 2016; Noohinejad *et al.*, 2015; Schoenleber, 2011; Schoenleber *et al.*, 2003).

The modulated structure suggests that the phase transition is dominated by evolution of internal torsional degrees of freedom ($\varphi^3 > 0^\circ$) within the biphenyl moieties [Fig. 4(a)]. The twists about the central C–C bond are significantly different for the two molecules where the torsional modulation of ‘A’ are 2-4 times larger than those of ‘B’ (dihedral angle: $|\varphi_A^3| = 15.6 \text{ deg}, 20.5 \text{ deg}$; $|\varphi_B^3| = 4.1 \text{ deg}, 9.3 \text{ deg}$). These torsions are described by highly anisotropic AMFs (u) along the three basis vectors where the maximum amplitude are along \mathbf{b} for the carbon atoms of biphenyl (Fig. 4 and Table S4 in supporting information). Notably, the rotations in the present structure are significantly larger than those reported for molecular biphenyl [$\varphi \simeq \pm 5.5 \text{ deg}$ in ref.(Petricek *et al.*, 1985; Baudour & Sanquer, 1983; Baudour & Sanquer, 1983)] but smaller than those in the low temperature superstructure of p -terphenyl and p -quarterphenyl [Maximum $\varphi_{\text{terphenyl, quarterphenyl}} \simeq 23 \text{ deg}$ in ref.(Rice *et al.*, 2013; Baudour *et al.*, 1976; Baudour *et al.*, 1978)]. Another distinctive property of the modulated structure is the unequal modulation for the two different moieties where $u_{\text{biphenyl}} > u_{\text{phenylalaninate}}$ (Table S4 in supporting information). Therefore, the variation in torsions φ^1 and ψ are smaller [Fig. 4(c),(d)]. A possible reason for the weaker modulations of the atoms around the chiral centers is the directional strong intermolecular N–

H...O bonds makes large intramolecular rotations unfavorable. Note that the observed changes in the rotations φ^2 [Fig. 4(b)] of molecule ‘A’ are predominantly described by strong modulations of the molecule’s biphenyl moiety. The asymmetry in rotations of individual molecules ($\Delta |\varphi^3| \approx 5$ deg) is determined by the disparate bonding environments of the biphenyl moieties where the inner rings are that are covalently bonded to amide groups while the outer interact weakly *via* C–H...H–C interactions with the phenyl rings of phenylalaninate groups (Fig. 4). Subsequently, the unequal values at the relevant *t*-sections of φ^3 are correlated to those of φ^2 [compare Fig. 4(a) and Fig. 4(b)] suggesting the chemical influence of the amide groups on the phenyl rings and *vice-versa*.

In the modulated structure, the biphenyl moieties in (AA)_n and (BB)_n stacks are tilted with respect to each other [Fig. 4(e)] which are parallel in phase I. These tilts ($\theta_{AA/BB}$) are of the order of the internal twists, φ^3 of the independent biphenyl moieties [compare Fig. 4(e) to Fig. 4(a)] The orientation between the biphenyl moieties within the (ABAB)_n stacks also vary with $\Delta\theta_{AA/BB} \simeq 12$ deg where the value is intermediate to φ_A^3 and φ_B^3 [compare Fig. 4(e) to Fig. 4(a)]. In addition, intermolecular distances between the biphenyl moieties within the stacks at the two *t*-sections are different and vary up to $\Delta d_{AA/BB} \simeq 0.05$ Å and $\Delta d_{ABAB} \simeq 0.02$ Å [Fig. 4(f)]. However, these variations in *d* are small compared to the molecular tilts, θ . It could therefore be argued that the dimerization of biphenyl molecular stacks below T_c are predominantly governed by distortion described by molecular rotations rather than intermolecular distances. On the other hand, intermolecular distances between aromatic rings of L-phenylalaninate vary similarly to the biphenyls albeit significantly smaller interstack rotations, $\theta < 3$ deg (Fig. S5 in supporting information).

The increased distortions are also accompanied by suppression of dynamic disorder below T_c . For example, the carbon atoms at ortho (C14, C16, C19, C23) and meta

(C13, C17, C20, C22) positions are strongly displaced (Fig. 4, Table S4 and S5 in supporting information). Subsequently, the ADPs are significantly reduced as compared to phase I (Fig. 4, Table S5 in supporting information). Notably, decrease of the ADPs (U_{eq}) from $T = 160$ K to $T = 100$ K is larger for those of molecule ‘A’ than those for ‘B’, while the square of the amplitude of modulations (u^2) are greater for ‘A’ than those for ‘B’ [compare Fig. 4(b) to Fig. 4(a)].

3.2. Competitive forces governing modulations

Structural studies in the 3D phase of molecular biphenyl have suggested that the ortho-hydrogen atoms are displaced away in the plane of the rings to minimize steric hindrance (Trotter, 1961; Hargreaves & Rizvi, 1962; Charbonneau & Delugeard, 1976). On the other hand, dynamic disorder predominantly governed by torsional vibrations around the long molecular axis (Petricek *et al.*, 1985) is predicted to balance the planar conformation of biphenyl favourable for crystal packing (Lenstra *et al.*, 1994). As short as 1.98 Å in phase I (Table 2), these contacts are shorter than the predicted values for twice van der Waals radius for hydrogen ($r = 1.1$ – 1.2 Å (Rowland & Taylor, 1996; Alvarez, 2013)). In the modulated structure, we observe that the distances between the ortho-hydrogen atoms are marginally but consistently larger than those in phase I (Table 2) that could suggest that the torsional modulations aid in minimization of the presumed steric hindrance below T_c (Dey *et al.*, 2022; Dey *et al.*, 2018).

A peculiar property of the modulated structure under discussion is the significant difference in the torsional amplitude φ^3 of the independent molecules. This aspect cannot be explained solely based on the intramolecular steric factors. Analysis of the crystal packing shows that each of these independent biphenyl moieties maintains close intermolecular CH...HC contacts with the phenyl rings of L-phenylalaninate in AB and BA fashion (Fig. 4). These distances are significantly longer (intermolecular

$d_{\text{H}\cdots\text{H}} \geq 2.4 \text{ \AA}$, Table 2) compared to the intramolecular H \cdots H distances. On the other hand, the aromatic rings of L-phenylalaninate interact with adjacent oxygen atoms of $-\text{COOCH}_3$ *via* C–H \cdots O hydrogen bonds (Fig. 4 and Table 2). These hydrogen bonds are weaker (Desiraju & Steiner, 2001) but highly directional ($\angle(\text{C}–\text{H}\cdots\text{O}) = 159\text{--}164 \text{ deg}$) with very little variation in the distances. Interestingly, those H \cdots H distances involving biphenyl moieties of ‘B’ are consistently smaller than those of ‘A’ in both phases (Table 2). We argue that in the presence of both the van der Waals interactions and weak C–H \cdots O bonds, the larger distortions of ‘A’ is favored by weaker CH \cdots HC interactions while that is suppressed in ‘B’. The four different values of intramolecular torsion φ^3 within the biphenyl moieties is distinctively governed by intra- and intermolecular non-bonded H \cdots H contacts as well as weak hydrogen bonds.

4. Conclusions

The single crystal to single crystal phase transition of 4-biphenylcarboxy-(L)-phenylalaninate below $T = 124 \text{ K}$ drives the 3D structure directly to a locked-in twofold superstructure. The commensurately modulated structure at $T = 100 \text{ K}$ is accompanied by pronounced amplitudes of torsion within biphenyl that are characteristic of modulated and superstructures of other polyphenyls. The phase transition temperature is significantly higher than that in biphenyl yet significantly smaller than for p-terphenyl and p-quarterphenyl. Consistent with the T_c , the maximum amplitude of torsion is also intermediate and in the order $\varphi_{\text{quarterphenyl}} \geq \varphi_{\text{terphenyl}} > \varphi_{4\text{-biphenylcarboxy-L-phenylalaninate}} > \varphi_{\text{biphenyl}}$.

Topologically separated, conformations of both the weaker C–H \cdots O bonds and stronger N–H \cdots O bonds are rigid and that underlines their role in stabilizing the crystal packing in both phases. A unique property of the present polyphenyl coupled amino acid ester is the distinctively unequal torsional amplitude ($\varphi_A > \varphi_B$) within the

independent molecules which is governed by multiple level of competitions involving unequal van der Waals constraints in presence of weak hydrogen bonds between the biphenyl and L-phenylalaninate moieties. The unusual nature of the phase transition is described by the fact that unequal displacive modulations of the two molecules are complimented by unequal suppression of the dynamic disorder of their atoms below T_c . This difference in the torsion as well as the phase transition conditions highlights how conjugation of polyphenyls can possibly be influenced by amino acid esters which in turn influences supramolecular assemblies.

Acknowledgements We thank Prof. Sreenivasan Ramakrishnan, Dr. Vaclav Petricek, Dr. Sitaram Ramakrishnan, Prof. Venkataramanan Mahalingam and Dr. Saumya Mukherjee for helpful comments and fruitful discussions. Financial support from SERB-DST (DST-SERB:PDF/2018/002502) and Alexander von Humboldt foundation is gratefully acknowledged.

Table 1. *Temperature dependence of lattice parameters and the components of the modulation wave vector, σ_1 and σ_3 . See Table S1 in supporting information for reflections used.*

T (K)	a (Å)	b (Å)	c (Å)	β (deg)	σ_1	σ_3	V (Å ³)
200(Sasmal <i>et al.</i> , 2019a)	5.0560(3)	8.6622(4)	42.242(3)	90.349(4)			1850.00(18)
160	5.0479(2)	8.6330(4)	42.1525(15)	90.513(3)			1836.87(13)
150	5.0498(7)	8.6161(8)	42.136(11)	90.607(11)			1833.2(5)
140	5.0484(6)	8.6093(7)	42.145(10)	90.661(10)			1831.6(5)
130	5.0451(7)	8.6014(8)	42.120(11)	90.713(11)			1827.6(6)
128	5.0446(7)	8.6002(8)	42.113(11)	90.723(11)			1826.9(6)
126	5.0440(6)	8.5992(7)	42.114(10)	90.720(9)			1826.5(5)
124	5.0443(6)	8.5978(7)	42.100(10)	90.733(9)	0.499(9)	0.51(7)	1825.7(5)
122	5.0440(7)	8.5970(7)	42.100(10)	90.745(10)	0.498(6)	0.49(4)	1825.5(5)
120	5.0433(7)	8.5984(7)	42.100(10)	90.746(10)	0.497(5)	0.52(3)	1825.5(5)
118	5.0441(7)	8.5958(8)	42.092(11)	90.764(10)	0.500(4)	0.50(3)	1824.8(5)
116	5.0432(6)	8.5926(7)	42.087(9)	90.775(9)	0.500(4)	0.51(3)	1823.6(5)
114	5.0422(6)	8.5923(7)	42.090(10)	90.787(10)	0.500(4)	0.53(3)	1823.3(5)
100	5.0377(2)	8.5898(3)	42.0432(14)	90.884(3)	0.5	0.5	1819.11(11)

Table 2. *Comparison of non-bonded hydrogen...acceptor and hydrogen...hydrogen distances (Å) involved in hydrogen bonds and steric factors in phase I (T_1) and phase II (T_2 ; $t = \frac{1}{4}; \frac{3}{4}$) respectively. Symmetry codes: Phase I- (i) $x - 1, y, z$; (ii) $x + 1, y, z$; (iii)*

$-x + 1, y + \frac{1}{2}, -z + 1$; (iv) $-x + 2, y - \frac{1}{2}, -z$. Phase II- (i) $x - 1, y, z, t$; (ii) $x + 1, y, z, t$; (iii)

Interaction class	Atom group labels	Phase	distances (Å)
N-H...O	H1n1a...O3a ⁱ	I	2.00
		II	1.97; 1.95
	H1n1b...O3b ⁱⁱ	I	2.00
		II	2.00, 1.98
C-H...O	H1c10a...O2a ⁱⁱⁱ	I	2.72
		II	2.72; 2.68
	H1c10b...O2b ^{iv}	I	2.78
		II	2.74; 2.73
Intra H...H	H1c14a...H1c19a	I	1.98
		II	2.08; 2.09
	H1c14b...H1c19b	I	1.98
		II	2.00; 1.99
	H1c16a...H1c23a	I	2.03
		II	2.10; 2.16
H1c16b...H1c23b	I	2.02	
	II	2.03; 2.06	
Inter H...H	H1c21a...H1c7b	I	2.59
		II	2.61; 2.56
	H1c21b...H1c7a ⁱⁱ	I	2.45
		II	2.39; 2.46

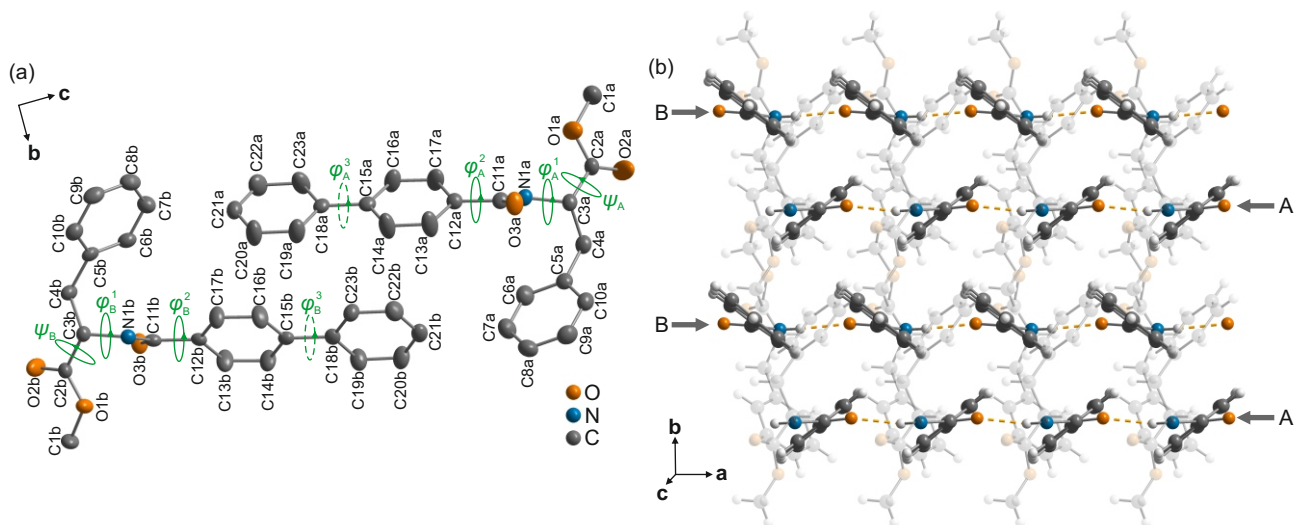


Fig. 1. (a) Two independent formula units of 4-biphenylcarboxy-(L)-phenylalaninate ($\text{C}_{23}\text{H}_{21}\text{NO}_3$) with atomic labels of non-hydrogen atoms ('a' and 'b' for molecule 'A' and 'B' respectively) in phase I at $T = 160$ K. $\varphi_{\text{A}}^1 = -130.1$ deg, $\varphi_{\text{B}}^1 = 56.1$ deg; $|\varphi_{\text{A}}^2| = 32.8$ deg, $|\varphi_{\text{B}}^2| = 30.8$ deg; $\varphi_{\text{A}}^3 = \varphi_{\text{B}}^3 = 0$ deg; $\psi_{\text{A}} = 36.4$ deg, $\psi_{\text{B}} = 36.2$ deg. Viewing direction along $[\bar{1}00]$. (b) View of corresponding layered structure along $[111]$ emphasizing biphenyl stacks $(AA)_n$ and $(BB)_n$ along \mathbf{a} , $(ABAB)_n$ along \mathbf{b} and $\text{N-H}\cdots\text{O}$ bonds (dashed orange) along $[\mp 100]$ directions. Phenyl rings of the ester groups (transparent) stack only along \mathbf{a} .

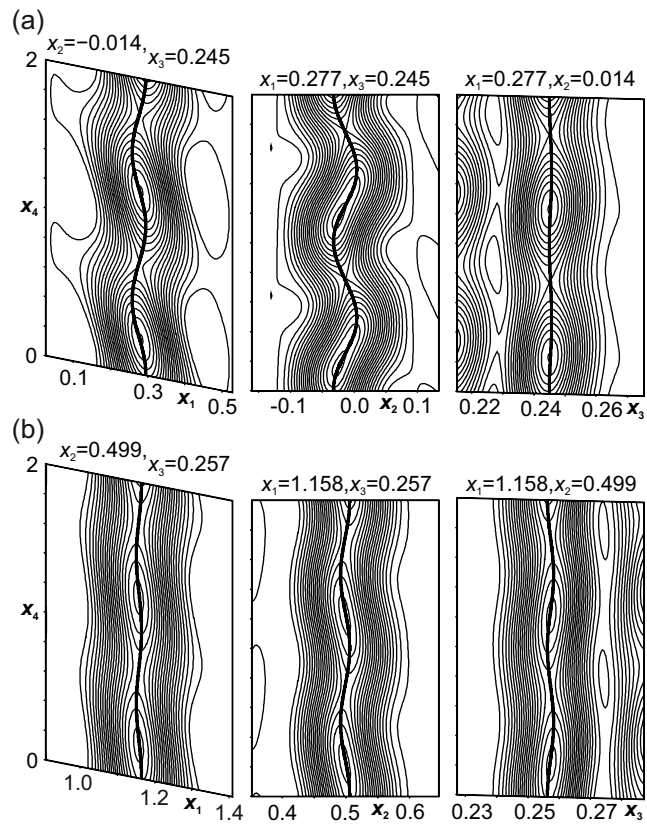


Fig. 2. (x_{si}, x_{s4}) -sections of Fourier map centered on carbon atoms (black) (a) C23a of molecule 'A' and (b) C23b of molecule 'B' respectively. The contour line and the width of the maps are $0.5 \text{ e}\text{\AA}^{-3}$ and 2.5 \AA respectively.

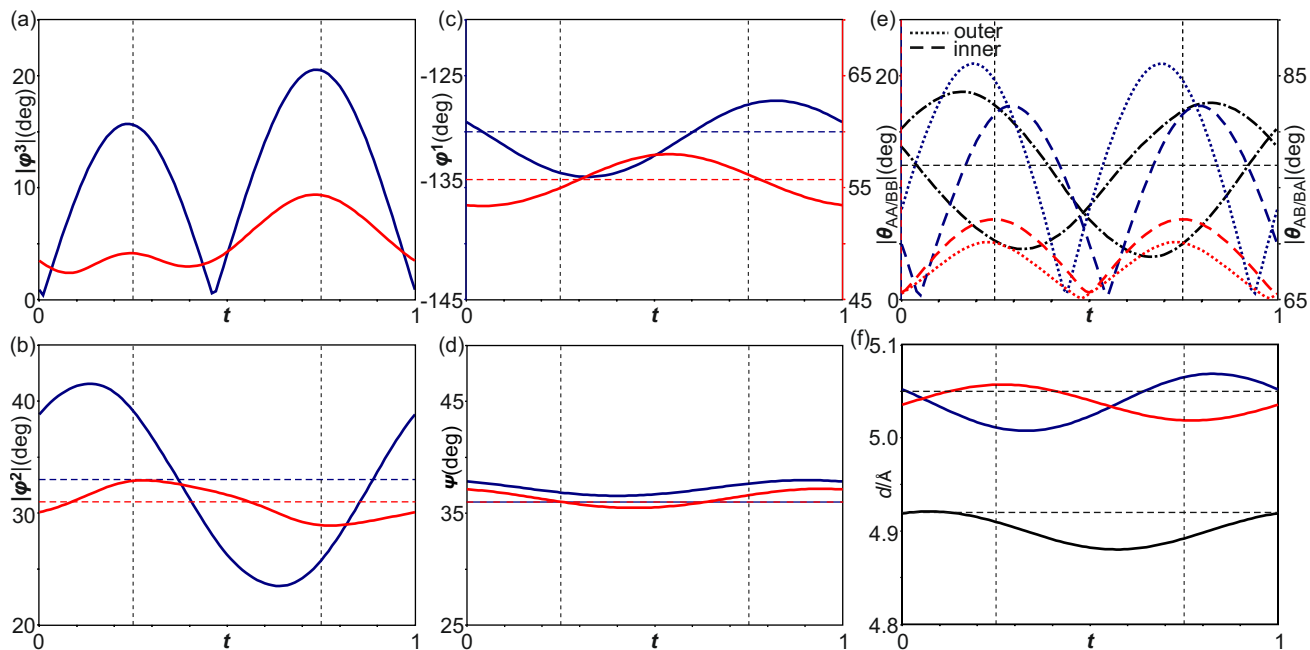


Fig. 3. t -plots of intramolecular rotations of molecule 'A' (blue) and 'B' (red) as well as intermolecular tilts and distances between stacks of 4-biphenylcarxy-(L)-phenylalaninate. (a) Dihedral angle, $|\varphi^3|$ represents internal torsion within biphenyl; (b) Dihedral angle, $|\varphi^2|$ represents torsion between the inner ring of biphenyl and the amide groups; (c) φ^1 represents torsion of the amide groups with respect to the $-\text{COOCH}_3$ groups; (d) ψ represent torsion of $-\text{COOCH}_3$ groups with respect to amide groups. (e) $|\theta_{AA/BB}|$ represent tilt between biphenyl rings of 'A' and 'A'ⁱⁱⁱ (blue); and of 'B' and 'B'ⁱⁱⁱ (red) and $|\theta_{AB/BA}|$ (dashed-dotted black curve) represent tilt between inner aromatic rings of biphenyl (bonded to amide groups) of 'A' and outer ring of 'B' and vice-versa. (f) Intermolecular distances (d) between biphenyl rings of 'A' and 'A'ⁱⁱⁱ (blue), between those of 'B' and 'B'ⁱⁱⁱ (red) and between those of 'A' and 'B' (black). Horizontal dashed lines represent those angles and distances in phase I ($|\varphi^3| = |\theta_{AA/BB}| = 0$ deg). Vertical dashed lines indicate t values corresponding to angles and distances in the 3D superstructure.

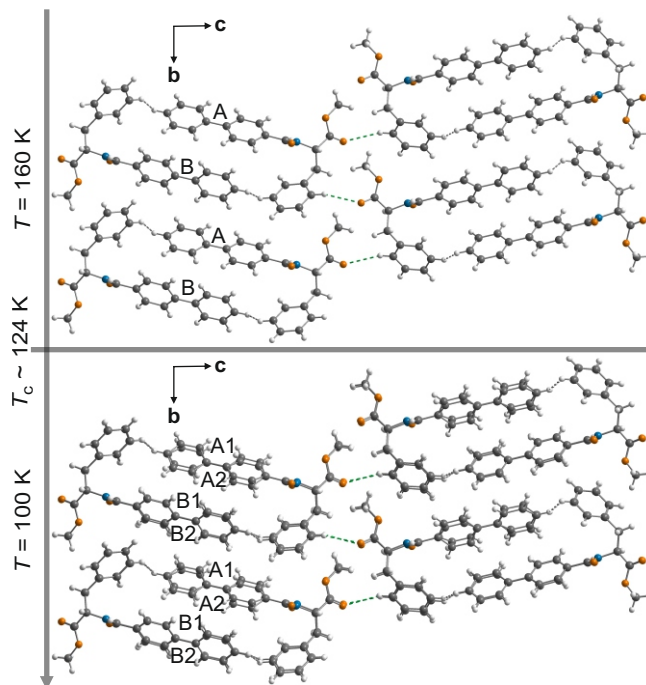


Fig. 4. Comparison of structures in phase I and phase II across the phase transition highlighting the effect of internal torsion (φ^3) within biphenyl on the stacking arrangements along **a**. The tilt between the biphenyl stacks, $\theta_{AA/BB}$ are different for the inner rings (bonded to amide rings) and the outer rings [corresponding values in *t*-plot in Fig. 4(e)]. See full unit cells in Fig. S6 in supporting information. View along $[\bar{1}00]$.

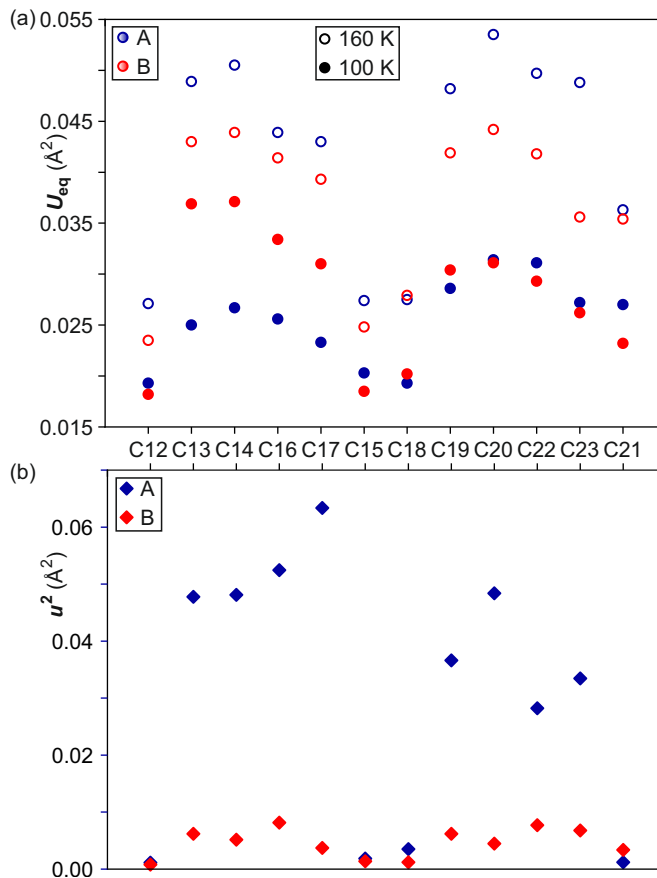


Fig. 5. Scatter plots of equivalent value of anisotropic ADPs (U_{eq}) and square of the amplitude of modulations (u^2) of the carbon atoms of biphenyl moieties (C12 through to C23, see Fig. 4.) of molecule 'A' (blue) and 'B' (red). (a) U_{eq} of the carbon atoms at $T = 160$ K (open circles) and at $T = 100$ K (full circles). (b) u^2 (diamonds) of the corresponding carbon atoms of molecule 'A' and 'B'. See Table S5 in supporting information.

References

- (2019). *CrysAlisPro Software system*. Rigaku Oxford Diffraction, Rigaku Corporation, Oxford, UK.
- Alvarez, S. (2013). *Dalton Trans.* **42**, 8617–8636.
- Bastiansen, O. (1949). *Acta Chem. Scand.* **3**, 408–414.
- Baudour, J. L., Delugeard, Y. & Cailleau, H. (1976). *Acta Crystallogr. B*, **32**, 150–154.
- Baudour, J. L., Delugeard, Y. & Rivet, P. (1978). *Acta Crystallogr. B*, **34**, 625–628.
- Baudour, J. L. & Sanquer, M. (1983). *Acta Crystallogr. B*, **39**, 75–84.
- Benkert, C. & Heine, V. (1987). *Phys. Rev. Lett.* **58**, 2232–2234.
- Benkert, C., Heine, V. & Simmons, E. H. (1987). *J. Phys. C: Solid State Phys.* **20**, 3337–3354.
- Bree, A. & Edelson, M. (1977). *Chem. Phys. Lett.* **46**, 500–504.
- Bree, A. & Edelson, M. (1978). *Chem. Phys. Lett.* **55**, 319–322.

- Buerkle, M., Viljas, J. K., Vonlanthen, D., Mishchenko, A., Schoen, G., Mayor, M., Wandlowski, T. & Pauly, F. (2012). *Phys. Rev. B*, **85**, 075417.
- Busing, W. R. (1983). *Acta Crystallogr. A*, **39**, 340–347.
- Cailleau, H., Moussa, F. & Mons, J. (1978). *Solid State Commun.* **31**, 521–524.
- Casalone, G., Mariani, C., Mugnoli, A. & Simonetta, M. (1968). *Mol. Phys.* **15**, 339–348.
- Charbonneau, G. P. & Delugeard, Y. (1976). *Acta Crystallogr. B*, **32**, 1420–1423.
- Charbonneau, G. P. & Delugeard, Y. (1977). *Acta Crystallogr. B*, **33**, 1586–1588.
- Cranney, M., Comtet, G., Dujardin, G., Kim, J. W., Kampen, T. U., Horn, K., Mamatkulov, M., Stauffer, L. & Sonnet, P. (2007). *Phys. Rev. B*, **76**, 075324.
- Desiraju, G. R. & Steiner, T. (2001). Oxford University Press, 1st ed.
- Dey, S., Schoenleber, A., Mondal, S., Ali, S. I. & van Smaalen, S. (2018). *Cryst. Growth Des.* **18**, 1394–1400.
- Dey, S., Schoenleber, A., Mondal, S., Prathapa, S. J., van Smaalen, S. & Larsen, F. K. (2016). *Acta Crystallogr. B*, **72**, 372–380.
- Dey, S., Schoenleber, A., van Smaalen, S., Morgenroth, W. & Larsen, F. K. (2022). *Chem. Eur. J.* **28**, e202104151.
- Ecolivet, C. & Sanquer, M. (1983). *J. Chem. Phys.* **78**, 6317–6324.
- Friedman, P. S., Kopelman, R. & Prasad, P. N. (1974). *Chem. Phys. Lett.* **24**, 15–17.
- Hargreaves, A. & Rizvi, S. H. (1962). *Acta Crystallogr.* **15**, 365–373.
- Hochstrasser, R. M., McAlpine, R. D. & Whiteman, J. D. (1973). *J. Chem. Phys.* **58**, 5078–5088.
- Ishibashi, Y. (1981). *J. Phys. Soc. Jpn.* **50**, 1255–1258.
- Janner, A. & Janssen, T. (1977). *Phys. Rev. B*, **15**, 643–658.
- Janssen, T., Chapuis, G. & de Boissieu, M. (2018). Oxford University Press, 2nd ed.
- Jeong, H., Li, H. B., Domulevicz, L. & Hihath, J. (2020). *Adv. Funct. Mater.* **30**, 2000615.
- Khatua, R., Sahoo, S. R., Sharma, S. & Sahu, S. (2020). *Synth. Met.* **267**, 116474.
- Lenstra, A. T. H., van Alsenoy, C., Verhulst, K. & Geise, H. J. (1994). *Acta Crystallogr. B*, **50**, 96–106.
- Mishchenko, A., Vonlanthen, D., Meded, V., Buerkle, M., Li, C., Pobelov, I. V., Bagrets, A., Viljas, J. K., Pauly, F., Evers, F., Mayor, M. & Wandlowski, T. (2010). *Nano Lett.* **10**, 156–163.
- Nespolo, M. (2019). *Acta Crystallogr. A*, **75**, 551–573.
- Noohinejad, L., Mondal, S., Ali, S. I., Dey, S., van Smaalen, S. & Schoenleber, A. (2015). *Acta Crystallogr.* **71**, 228–234.
- Oniwa, K., Kanagasekaran, T., Jin, T., Akhtaruzzaman, M., Yamamoto, Y., Tamura, H., Hamada, I., Shimotani, H., Asao, N., Ikeda, S. & Tanigaki, K. (2013). *J. Mater. Chem. C*, **1**, 4163–4170.
- Palatinus, L. & Chapuis, G. (2007). *J. Appl. Crystallogr.* **40**, 786–790.
- Parlinski, K., Schranz, W. & Kabelka, H. (1989). *Phys. Rev. B*, **39**, 488–494.
- Petricek, V., Coppens, P. & Becker, P. (1985). *Acta Crystallogr. A*, **41**, 478–483.
- Petricek, V., Dusek, M. & Palatinus, L. (2014). *Z. Kristallogr.* **229**, 345–352.
- Petricek, V., Dusek, M. & Plasil, J. (2016). *Z. Kristallogr.* **231**, 583–599.
- Petricek et al, V., (2022). JANA2020. Institute of Physics, Prague, Czech Republic.
- Pinheiro, C. B. & Abakumov, A. M. (2015). *IUCrJ*, **2**, 137–154.
- Popelier, P. L. A., Maxwell, P. I., Thacker, J. C. R. & Alkorta, I. (2019). *Theor. Chem. Acc.* **138**, 12.
- Ramakrishnan, S., Schoenleber, A., Huebschle, C. B., Eisele, C., Schaller, A. M., Rekiş, T., Bui, N. H. A., Feulner, F., van Smaalen, S., Bag, B., Ramakrishnan, S., Tolkiehn, M. & Paulmann, C. (2019). *Phys. Rev. B*, **99**, 195140.
- Rekiş, T., Schoenleber, A., Noohinejad, L., Tolkiehn, M., Paulmann, C. & van Smaalen, S. (2021). *Cryst. Growth Des.* **21**, 2324–2321.

- Rice, A. P., Tham, F. S. & Chronister, E. L. (2013). *J. Chem. Crystallogr.* **43**, 14–25.
- Rowland, R. S. & Taylor, R. (1996). *J. Phys. Chem.* **100**, 7384–7391.
- Saito, K., Atake, T. & Chihara, H. (1985). *J. Chem. Thermodynamics*, **17**, 539–548.
- Sasmal, S., Nandi, S. K., Kumar, S. & Haldar, D. (2019a). *ChemistrySelect*, **4**, 11172–11176.
- Sasmal, S., Podder, D., Debnath, M., Nandi, S. K. & Haldar, D. (2019b). *ChemistrySelect*, **4**, 10302–10306.
- Schoenleber, A. (2011). *Z. Kristallogr.* **226**, 499–517.
- Schoenleber, A., Meyer, M. & Chapuis, G. (2001). *J. Appl. Crystallogr.* **34**, 777–779.
- Schoenleber, A., Pattison, P. & Chapuis, G. (2003). *Z. Kristallogr.* **218**, 507–513.
- Seechurn, C. C. C. J., Kitching, M. O., Colacot, T. J. & Snieckus, V. (2012). *Angew. Chem. Int. Ed.* **51**, 5062–5085.
- van Smaalen, S. (2012). Oxford University Press, 1st ed.
- van Smaalen, S., Campbell, B. J. & Stokes, H. T. (2013). *Acta Crystallogr. A*, **69**, 75–90.
- Steed, K. M. & Steed, J. W. (2015). *Chem. Rev.* **115**, 2895–2933.
- Stokes, H. T., Campbell, B. J. & van Smaalen, S. (2011). *Acta Crystallogr. A*, **67**, 45–55.
- Suzuki, H. (1959). *Bull. Chem. Soc. Jpn*, **32**, 1340–1350.
- Trotter, J. (1961). *Acta Crystallogr.* **14**, 1135–1340.
- Vonlanthen, D., Mishchenko, A., Elbing, M., Neuburger, M., Wandlowski, T. & Mayor, M. (2009). *Angew. Chem. Int. Ed.* **48**, 8886–8890.
- Wagner, T. & Schoenleber, A. (2009). *Acta Crystallogr. B*, **65**, 249–268.
- Wakayama, N. I. (1981). *Chem. Phys. Lett.* **83**, 413–417.
- Wei, J., Liang, B., Duan, R., Cheng, Z., Li, C., Zhou, T., Yi, Y. & Wang, Y. (2016). *Angew. Chem. Int. Ed.* **55**, 15589–15593.
- de Wolff, P. M. (1974). *Acta Crystallogr. A*, **30**, 777–785.
- Yamamura, Y., Saito, K., Ikemoto, I. & Sorai, M. (1998). *J. Phys.: Condens. Matter*, **10**, 3359–3366.

Synopsis

Coupled molecule of 4-biphenylcarboxy-(L)-phenylalaninate undergoes normal to commensurately modulated phase transition at $T_c \sim 124$ K that is characterized by torsional modulation typical of modulated structures and superstructures of polyphenyls yet unusual owing to asymmetric and unequal rotations governed by intramolecular and intermolecular constraints. The transition is presumably governed by significant suppression of atomic displacement parameters correlated to evolution of amplitude of atomic modulation functions.

Supporting information

Asymmetric rotations and dimerization driven by normal to modulated phase transition in 4-biphenylcarboxy coupled L-phenylalaninate

Somnath Dey^{a,b*}, Supriya Sasmal^a, Saikat Mondal^a, Santosh Kumar^a, Rituparno Chowdhury^a, Debashrita Sarkar^a, C. Malla Reddy^a, Lars Peters^b, Georg Roth^b and Debasish Haldar^a

^a*Department of Chemical Sciences, Indian Institute of Science Education and Research (IISER) Kolkata, Mohanpur 741246, India,*

^b*Institute of Crystallography, RWTH Aachen University, Jägerstraße 17-19, 52066 Aachen, Germany*

E-mail: dey@ifk.rwth-aachen.de

Contents

Details of structure refinements

Powder X-ray diffraction experiments

Supplementary Figures S1–S7

Supplementary Table S1–S7.

Details of structure refinements of different modulated structure models

Structure refinements have been performed using JANA2006¹ and JANA2020². Structural model at $T = 160$ K has been used as an initial model for the basic structure of the modulated structure at $T = 100$ K. All atoms were set to isotropic for displacement parameters and the model was refined against main reflections [$R_F^{obs}(m=0) = 0.0723$]. In the next step, first order harmonic for displacive modulation was described for all atoms and an incommensurate (IC) model was refined against main and satellite reflections. Refinement led to improved fit to the main reflections [$R_F^{obs}(m=0) = 0.0586$, $R_F^{obs}(m=1) = 0.1215$]. Refinement of the anisotropic atomic displacement parameters (ADPs) of all non-hydrogen atoms resulted in significant improvement to the residual values [IC model A: $R_F^{obs}(m=0) = 0.0374$, $R_F^{obs}(m=1) = 0.0771$] and residual features ($\Delta\rho_{min}/\Delta\rho_{max}$) decreased from $-0.68/1.23$ eÅ⁻³ to $-0.33/0.31$ eÅ⁻³. However, ADPs of four non-hydrogen atoms were found to be non-positive definite. Further test by describing first order harmonic for ADP modulation for all non-hydrogen atoms model led to improvement of the residual values [IC model A: $R_F^{obs}(m=0) = 0.0363$, $R_F^{obs}(m=1) = 0.0677$] but ADPs of 11 non-hydrogen atoms were found to be non-positive definite along certain t -sections. This model was discarded for further analysis.

In the next step, IC model A was used as a starting model to describe three commensurate (C) models by fixing the initial phase of the modulation, $t_0 = 0$, $\frac{1}{4}$ and $\frac{1}{8}$ respectively. The former two t_0 values correspond to $2a \times b \times 2c$ superstructure in 3D with monoclinic symmetry $B2_1$ while the later correspond to a superstructure with triclinic $B1$ symmetry. Restrictions on t_0 values also impose constraints on the refinable variables corresponding to atomic modulation functions (AMFs). These restrictions follow the argument that the total number of refinable parameters in the equivalent 3D superstructure and their (3+1)D commensurately modulated structural models must be equal. In the present case, either sin or cos waves can be refined for structural models with $t_0 = 0$ and $\frac{1}{4}$ because the point group symmetry is same in their corresponding 3D superstructure models. On the other hand, assumed monoclinic to triclinic distortion in the 3D superstructure (space group $B1$) corresponding to (3+1)D C model with $t_0 = \frac{1}{8}$ can be derived by using both components of the Fourier series. It must be noted that such restrictions on sin and cos waves cannot be formally imposed on the AMFs of hydrogen atoms in JANA2006 and JANA2020 as their modulations are fully determined by geometrical conditions of the riding model. $t_0 = \frac{1}{4}$ yielded the best fit to the diffraction data (Table S3) with reduced number of parameters as compared to the IC model A (compare $N_{C,t_0=0.25} = 649$ to $N_{IC,model A} = 811$). Most importantly, ADPs of all non-hydrogen atoms are positive definite.

Notably, the residual values of the IC model as well as the C model at $t_0 = \frac{1}{8}$ is marginally

smaller than for the C model at $t_0 = \frac{1}{4}$. Assuming all the three models should fit similarly to the diffraction data for equivalent descriptions of structural models further tests included attempts to refine the IC model and C model at $t_0 = \frac{1}{8}$ with reduced number of parameters (= 649) similar to $t_0 = \frac{1}{4}$. Refinements led to worse fit with large R -values (Table S3).

In the final step, all reflections were averaged in monoclinic symmetry corresponding to $t_0 = 0$. One parameter corresponding to isotropic extinction correction was refined. Finally, fractional co-ordinates and AMFs for hydrogen atoms belonging to N–H groups involved in strong hydrogen bonds improved the fit to the diffraction data marginally ($R_F^{obs} = 0.0419$ in Table S2).

Additional refinement was performed including first order harmonic for anisotropic ADPs of all non-hydrogen atoms. Refinement of this model with additional 324 parameters converged with marginal improvement of R_F^{obs} (= 0.0406) values. However, the residual density $\Delta\rho_{min}/\Delta\rho_{max}$ remained unchanged [compare $-0.26/0.28$ e/Å³ to $-0.25/0.29$ e/Å³] and 306 parameters refined to values within three times their standard uncertainties. The model was therefore discarded. Thus the superspace approach reduced the total numbers of refinable parameters by ~ 33 %.

Additional X-ray diffraction experiments

Powder X-ray diffraction experiments were performed on thoroughly ground powder of the compound at ambient conditions using a Rigaku SmartLab with a CuK α radiation. JANA2006 was used to index the diffraction patterns. For reference, lattice parameters at ambient conditions were obtained from single crystal X-ray diffraction (SCXRD) experiment at ambient conditions (Table S7). The PXRD pattern could not be indexed using the lattice parameters as obtained from the SCXRD data [Fig. S7(a)] that suggest that the compound undergoes phase transition upon grinding. Lattice parameters were calculated employing the singular value decomposition (SVD)-Index algorithm in TOPAS^{3,4}. The PXRD pattern could be indexed using a primitive triclinic cell (Cell 1) with unit cell volume comparable to that of single crystal [Table S7, Fig. S7(b)]. Another triclinic cell (Cell 2) could also describe the pattern [Fig. S7(c)]. Le Bail refinements of the patterns against both the cells resulted in similar residual values (Table S7). However, Cell 1 fits better to the PXRD than Cell 2 [compare inset plots of Fig. S7(b) and Fig. S7(c)]. In addition, the unit cell volume of Cell 2 is larger than 7.5 % to that of the single crystal that implies different density of the ground material.

Based on this difference of phases between single crystals (monoclinic structure) and pulverised material (triclinic structure), T -dependent PXRD experiments to complement the single crystal to single crystal phase transition in this material was not pursued.

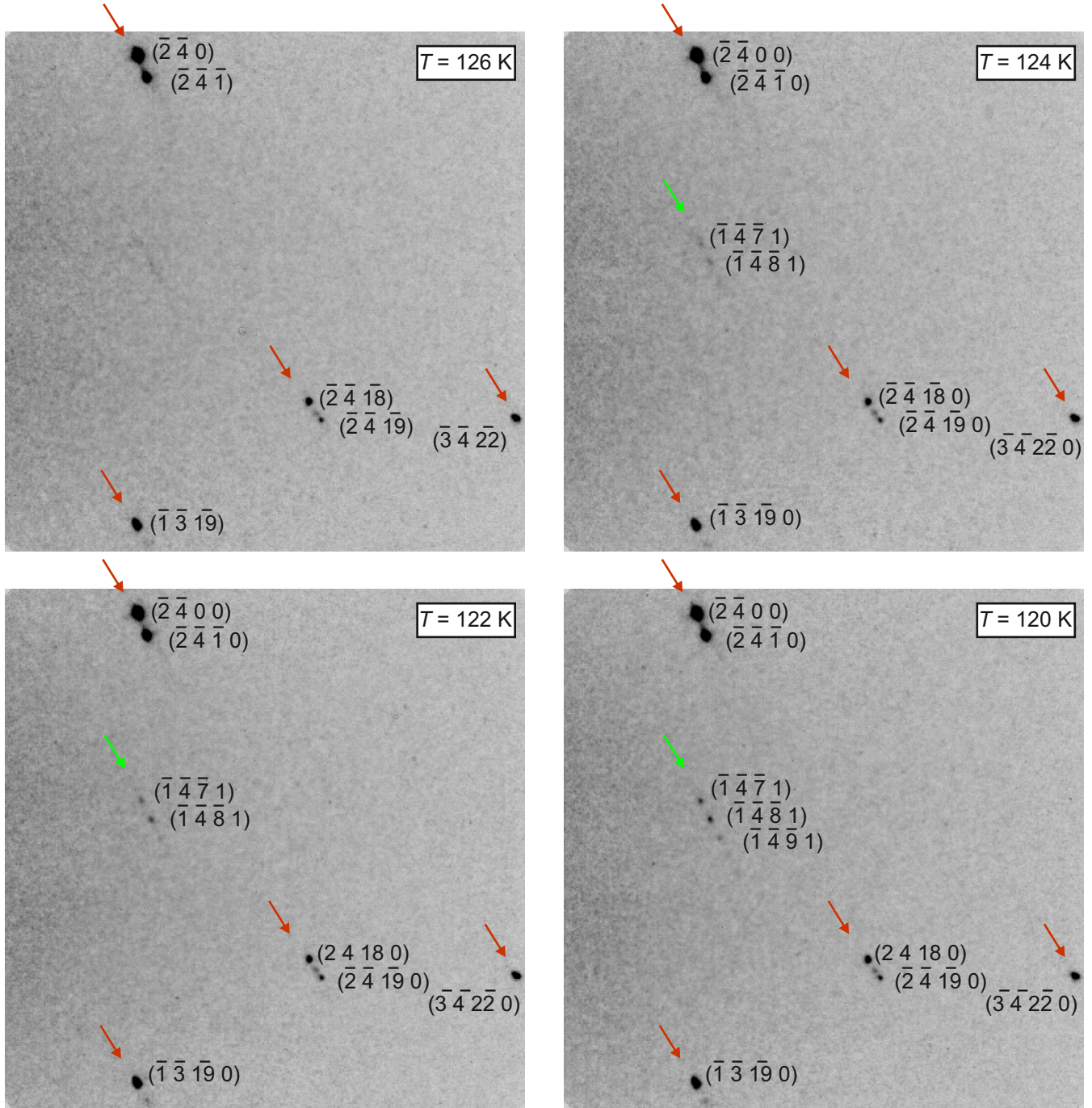


Figure S1: Diffraction images across the normal (phase I) to commensurately modulated (phase II) phase transition. Red arrows depict Bragg peaks in phase I and main Bragg peaks in phase II. The satellites are diffuse at $T = 124$ K (green arrow) that becomes stronger at lower temperatures. Reflections at $T = 126$ K are indexed using three integers (hkl) and at $T_c = 124$ K and lower temperatures by four integers $(hkml)$, where $m = 0$ and $m = 1$ for main and satellite reflections respectively. Image resolution range in $d \sim 2.2$ to 1.1 Å.

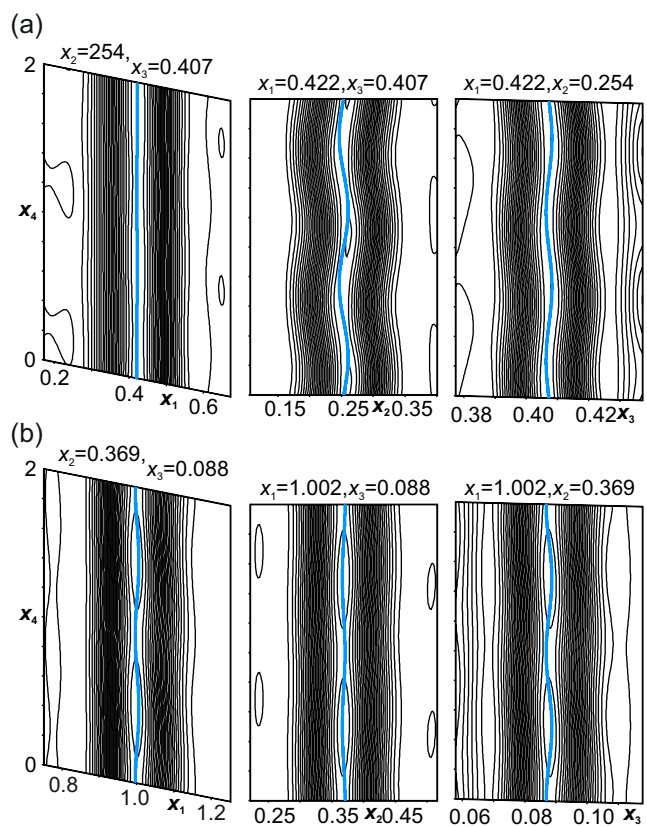


Figure S2: (x_{si}, x_{s4}) -sections of Fourier map centered on nitrogen atoms (light blue) of amide groups (a) atom N1a of molecule 'A' and (b) atom N1b of molecule 'B'. The contour line and the width of the maps are $0.5 \text{ e}\text{\AA}^{-3}$ and 2.5 \AA respectively.

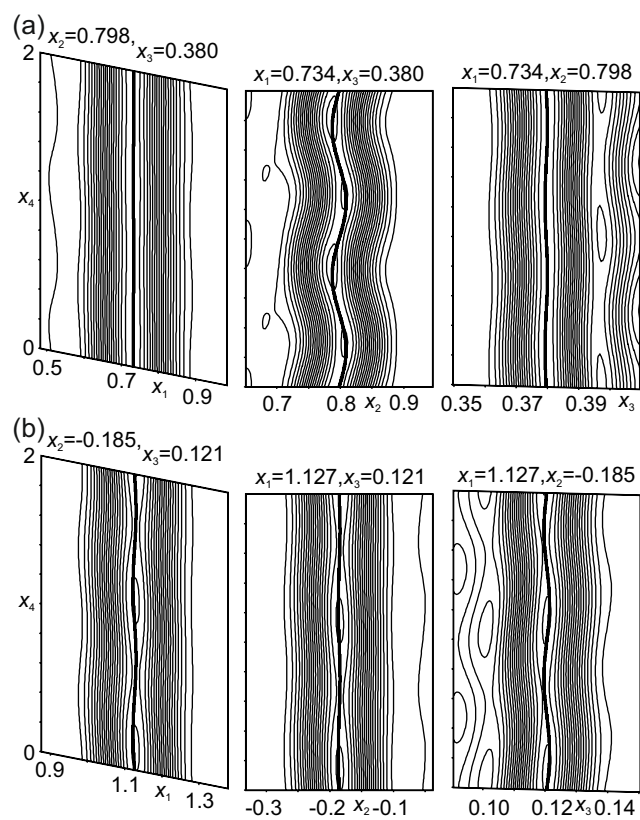


Figure S3: (x_{si}, x_{s4}) -sections of Fourier map centered on carbon atoms (black) (a) C8a of molecule 'A' and (b) C8b of molecule 'B' respectively belonging to the phenyl ring of L-phenylalaninate moieties. The contour line and the width of the maps are $0.5 \text{ e}\text{\AA}^{-3}$ and 2.5 \AA respectively.

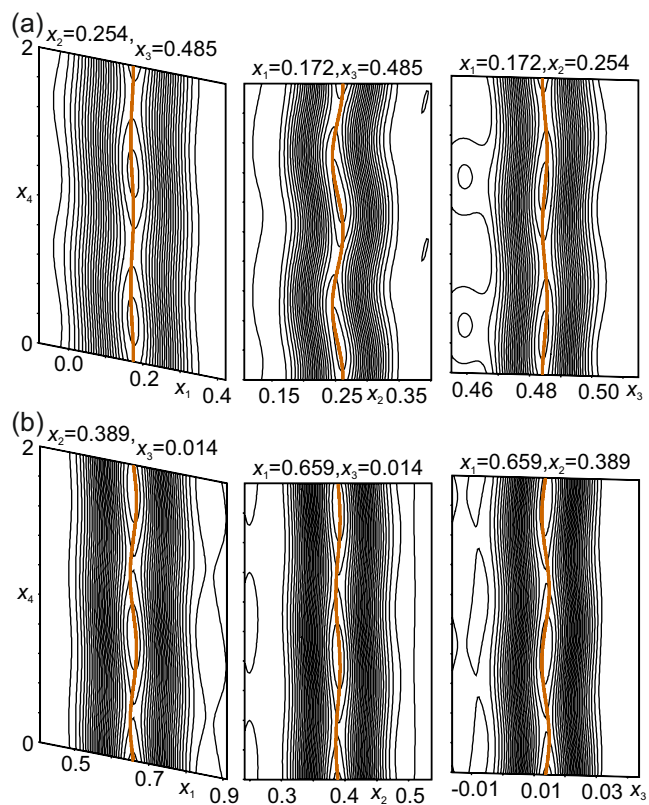


Figure S4: (a) and (b) (x_{s_i}, x_{s_4}) -sections of Fourier map centered on oxygen atoms (orange) O2a of molecule 'A' and O2b of molecule 'B' respectively belonging to carboxylate groups of L-phenylalaninate moieties. The contour line and the width of the maps are $0.5 \text{ e}\text{\AA}^{-3}$ and 2.5 \AA respectively.

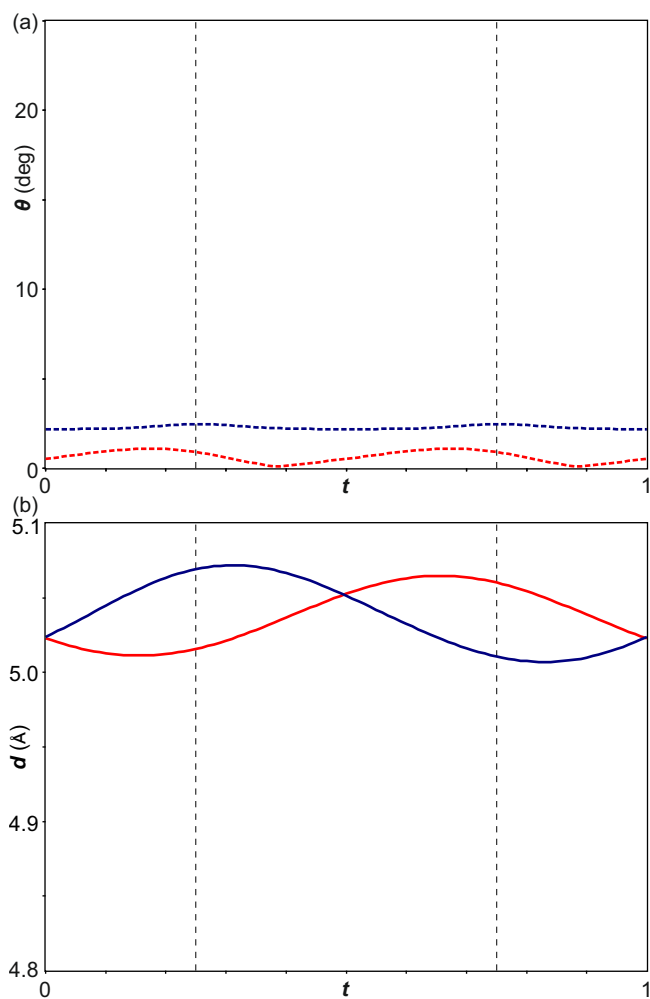


Figure S5: t -plots of (a) angle (θ) and (b) distances (d) describing the tilt and intermolecular distances between phenyl rings of L-phenylalaninate moieties within stacks along \mathbf{a} .

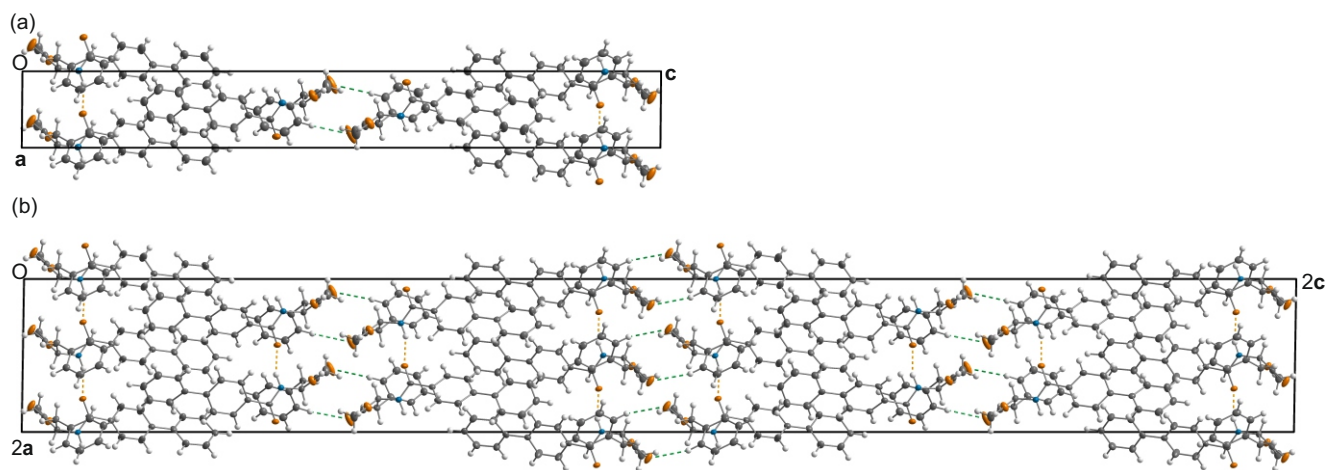


Figure S6: Crystal packing of 4-biphenylcarboxy-(L)-phenylalaninate at (a) $T = 160$ K (phase I) and (b) $2a \times b \times 2c$ superstructure at $T = 100$ K (phase II). Dashed orange lines depict linear N-H...O hydrogen bonds along $[\mp 100]$ directions, while green dashed lines represent C-H...O hydrogen bond dimers. Displacement ellipsoids are cut at 50% probability level. Viewing direction along $[010]$.

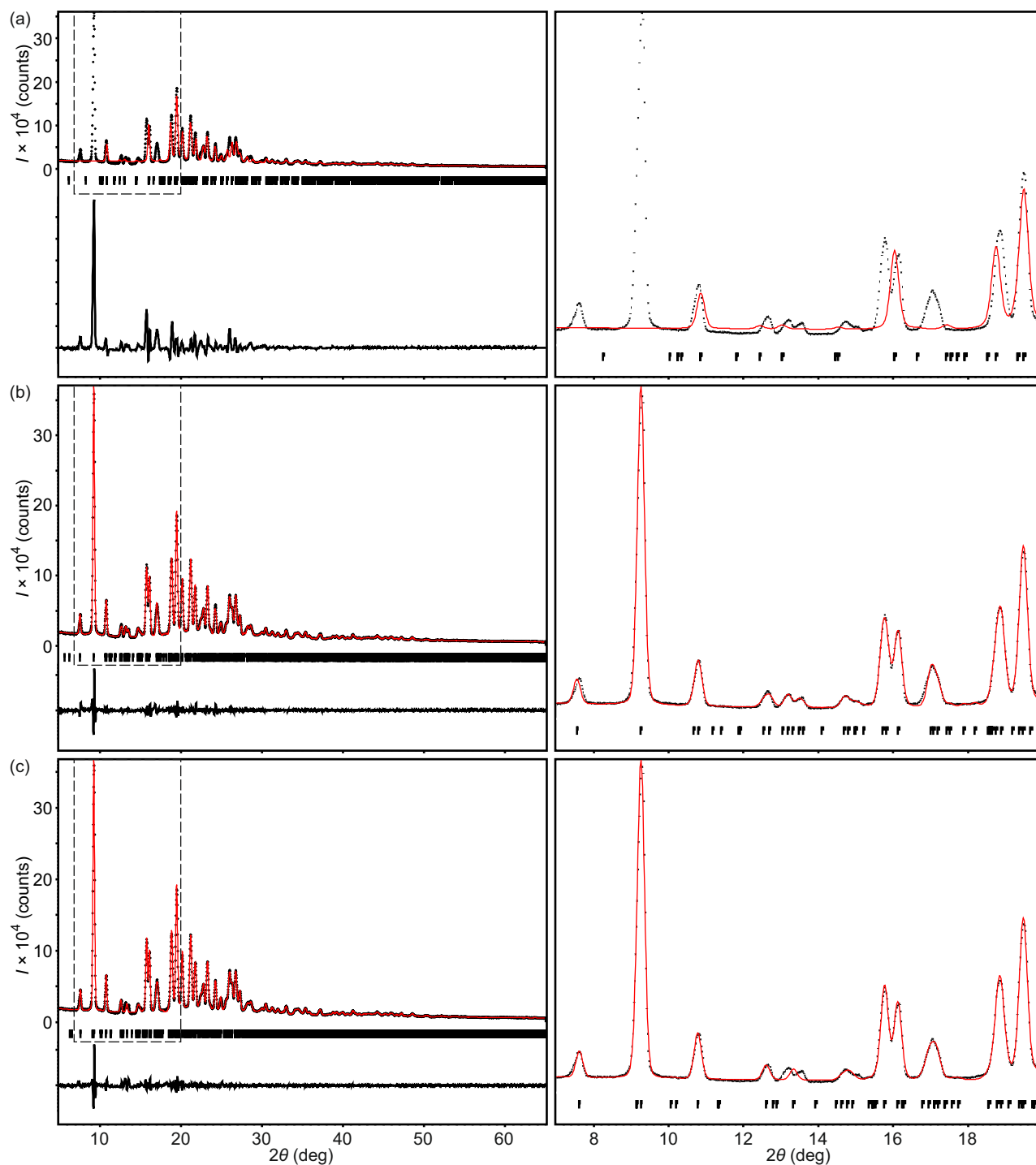


Figure S7: Comparison of fit of the experimental powder X-ray diffraction pattern to (a) as obtained unit cell from SCXRD, (b) Calculated unit cell 1 with volume 1901 \AA^3 and (c) calculated unit cell with volume 2029 \AA^3 . Experimental pattern, calculated profile and difference are given in black cross points, red curve and black curve respectively. The insets in $2\theta = 7\text{-}20$ deg are given in the right column corresponding to the area (dashed rectangle) in left.

Table S1: Technical details of SCXRD measurements and number of reflections used for calculation of lattice parameters and components of modulation wave vector, \mathbf{q} .

T (K)	Number of runs	Number of images	d_{max} (Å)	Number of reflections
160	27	1345	0.84	3437
150	9	45	0.84	130
140	9	45	0.84	140
130	9	45	0.84	136
128	9	45	0.84	134
126	9	45	0.84	139
124	9	45	0.84	135
122	9	45	0.84	147
120	9	45	0.84	152
118	9	45	0.84	149
116	9	45	0.84	159
114	9	45	0.84	161
100	26	1486	0.84	3948

Table S2: Experimental and crystallographic data

Crystal data		
Chemical formula		$\text{C}_{23}\text{H}_{21}\text{NO}_3$
M_r		359.42
Temperature (K)	160	100
Crystal system	Monoclinic <i>b</i> -unique	Monoclinic <i>b</i> -unique
<i>a</i> , <i>b</i> , <i>c</i> (Å)	5.0479(2), 8.6330(4), 42.1525(15)	5.0377(2), 8.5898(3), 42.0432(14)
β (deg)	90.513(3)	90.884(3)
<i>V</i> (Å ³)	1836.87(13)	1819.11(11)
Wave vector (q)	–	$\frac{1}{2}\mathbf{a}^* + \frac{1}{2}\mathbf{c}^*$
Space group	$P2_1$	–
Superspace group	–	$P2_1(\sigma_1 0 \sigma_3)0$
Commensurate section	–	$t_0 = \frac{1}{4}$
Supercell	–	$2a \times b \times 2c$
Supercell space group	–	$B2_1$
Diffraction data		
Wavelength		CuK α
<i>d</i> (Å)	0.84	0.84
$\Delta\omega$ (deg)	1	1
Absorption correction		multiscan
Criterion of observability		$I > 3\sigma(I)$
Unique reflections		
all (obs/all)	4219/4555	5940/8898
<i>m</i> = 0 (obs/all)	–	4150/4390
<i>m</i> = 1 (obs/all)	–	1790/4508
R_{int} (obs/all)	0.0200/0.0202	0.0248/0.0274
<i>GoF</i> (obs/all)	1.57/1.54	1.60/1.40
R_F^{obs}/wR_F^{all}		
all (obs/all)	0.0393/0.0492	0.0419/0.0526
<i>m</i> = 0 (obs/all)	–	0.0368/0.0460
<i>m</i> = 1 (obs/all)	–	0.0791/0.1191
$\Delta\rho_{min}/\Delta\rho_{max}$ (e/Å ³)		-0.26/0.28
No. of parameters	494	662
H-atom treatment	mixed	mixed
Twin law	$2 \parallel \mathbf{a}$	$2 \parallel \mathbf{a}$
Twin volumes	0.9760(8)/0.0240(8)	0.9758(7)/0.0242(7)

Table S3: Statistical parameters (R_F^{obs} , $wR_{F^2}^{all}$) of the (3+1)D incommensurately modulated (IC) and commensurately modulated (C) refinements of models with different values of the phase t_0 . Number of reflections (obs/all) used in the refinements are averaged for the lowest triclinic point group symmetry: (m=0) = 4911/5241, (m=11) = 2031/5537. Space group (SG) symmetries of the equivalent 3D superstructures corresponding to different C structures are given which for the IC structure is meaningless.

	IC		$t_0 = 0$	$t_0 = \frac{1}{8}$		$t_0 = \frac{1}{4}$
SG	–		$B2_1$	$B1$		$B2_1$
No. of parameters	811	649	649	811	649	649
GoF (obs/all)	1.55/1.35	2.93/2.56	2.68/2.38	1.56/1.33	2.04/1.81	1.55/1.35
$(R_F^{obs}(\text{all}))$	0.0428	0.0745	0.0691	0.0428	0.0566	0.0433
$wR_{F^2}^{all}(\text{all})$	0.0539	0.1035	0.0961	0.0533	0.0731	0.0547
$R_F^{obs}(m = 0)$	0.0381	0.0424	0.0401	0.0384	0.0406	0.0384
$wR_{F^2}^{all}(m = 0)$	0.0473	0.0515	0.0492	0.0475	0.0498	0.0476
$R_F^{obs}(m = 1)$	0.0777	0.3119	0.2838	0.0758	0.1750	0.0800
$wR_{F^2}^{all}(m = 1)$	0.1232	0.3174	0.3653	0.1166	0.2402	0.1280
$\Delta\rho_{min}/\Delta\rho_{max}$ (e/Å ³)	-0.33/0.31	-1.28/1.30	-1.04/1.09	-0.31/0.30	-0.79/0.84	-0.36/0.30
-ve ADPs	4	4	1	none	2	none
correlations > 0.6	1	20	1	98	247	1

Table S4: Components of the amplitude of atomic modulation functions ($|u_x|$, $|u_y|$ and $|u_z|$) along the three basis vectors **a**, **b** and **c** respectively for molecules A and B.

Atom	$ u_x $ (Å)		$ u_y $ (Å)		$ u_z $ (Å)	
	A	B	A	B	A	B
C1	0.0015	0.0086	0.0996	0.0198	0.0340	0.0092
O1	0.0070	0.0050	0.0670	0.0120	0.0294	0.0071
C2	0.0156	0.0166	0.0739	0.0129	0.0319	0.0198
O2	0.0181	0.0433	0.0721	0.0283	0.0311	0.0483
C3	0.0121	0.0081	0.0498	0.0077	0.0336	0.0134
C4	0.0408	0.0045	0.0730	0.0112	0.0340	0.0172
C5	0.0348	0.0070	0.0610	0.0077	0.0265	0.0244
C6	0.0242	0.0010	0.0876	0.0009	0.0290	0.0311
C7	0.0045	0.0066	0.0945	0.0002	0.0219	0.0286
C8	0.0040	0.0196	0.0936	0.0112	0.0172	0.0378
C9	0.0217	0.0388	0.0910	0.0361	0.0328	0.0563
C10	0.0337	0.0136	0.0515	0.0198	0.0328	0.0357
N1	0.0030	0.0247	0.0610	0.0180	0.0399	0.0387
O3	0.0055	0.0045	0.0936	0.0249	0.0294	0.0345
C11	0.0025	0.0035	0.0129	0.0155	0.0282	0.0189
C12	0.0171	0.0141	0.0137	0.0120	0.0256	0.0210
C13	0.1083	0.0171	0.1898	0.0636	0.0029	0.0433
C14	0.1098	0.0146	0.1898	0.0584	0.0027	0.0391
C15	0.0191	0.0257	0.0266	0.0180	0.0277	0.0202
C16	0.1501	0.0821	0.1623	0.0352	0.0597	0.0130
C17	0.1657	0.0539	0.1787	0.0283	0.0631	0.0029
C18	0.0237	0.0247	0.0275	0.0103	0.0467	0.0219
C19	0.1264	0.0640	0.1366	0.0455	0.0446	0.0042
C20	0.1446	0.0423	0.1580	0.0507	0.0500	0.0105
C21	0.0081	0.0332	0.0060	0.0258	0.0332	0.0399
C22	0.0972	0.0463	0.1349	0.0567	0.0244	0.0483
C23	0.0922	0.0348	0.1572	0.0618	0.0160	0.0416

Table S5: Equivalent value of the ADP tensors, (U_{eq}) of atoms of the biphenyl moieties at $T = 160$ K (phase I) and $T = 100$ K (phase II); and the sum of the square of the amplitudes of their atomic modulation functions along three basis vectors (u^2) for molecules A and B . $u^2 = (u_x)^2 + (u_y)^2 + (u_z)^2$.

Atom label	Molecule	$U_{eq,PhaseI}$ (\AA^2)	$U_{eq,PhaseII}$ (\AA^2)	u^2 (\AA^2)
C12	A	0.0271	0.0193	0.0011
	B	0.0235	0.0182	0.0008
C13	A	0.0489	0.0250	0.0478
	B	0.0430	0.0369	0.0062
C14	A	0.0505	0.0267	0.0481
	B	0.0439	0.0371	0.0051
C15	A	0.0274	0.0203	0.0018
	B	0.0248	0.0185	0.0014
C16	A	0.0439	0.0256	0.0525
	B	0.0414	0.0334	0.0081
C17	A	0.0430	0.0233	0.0634
	B	0.0393	0.0310	0.0037
C18	A	0.0275	0.0193	0.0035
	B	0.0279	0.0202	0.0012
C19	A	0.0482	0.0286	0.0366
	B	0.0419	0.0304	0.0062
C20	A	0.0535	0.0314	0.0484
	B	0.0442	0.0311	0.0045
C21	A	0.0363	0.0270	0.0012
	B	0.0354	0.0232	0.0034
C22	A	0.0497	0.0311	0.0282
	B	0.0418	0.0293	0.0077
C23	A	0.0488	0.0272	0.0335
	B	0.0356	0.0262	0.0068

Table S6: Comparison of interatomic bond distances (\AA) of molecules A and B in phase I ($T = 160$ K) and phase II ($T = 100$ K).

Atom groups	phase I		phase II			
	A	B	A		B	
			$t = \frac{1}{4}$	$t = \frac{3}{4}$	$t = \frac{1}{4}$	$t = \frac{3}{4}$
C1–O1	1.45	1.45	1.44	1.45	1.45	1.45
O1–C2	1.31	1.33	1.32	1.32	1.33	1.33
C2–O2	1.18	1.20	1.20	1.19	1.20	1.21
C2–C3	1.52	1.53	1.52	1.52	1.52	1.52
C3–C4	1.53	1.55	1.54	1.54	1.55	1.56
C4–C5	1.51	1.51	1.50	1.51	1.51	1.51
C5–C6	1.39	1.40	1.38	1.39	1.39	1.40
C6–C7	1.39	1.38	1.38	1.38	1.38	1.38
C7–C8	1.37	1.38	1.39	1.40	1.38	1.38
C8–C9	1.38	1.39	1.38	1.38	1.40	1.39
C9–C10	1.39	1.40	1.39	1.39	1.38	1.38
C10–C5	1.39	1.38	1.40	1.39	1.39	1.39
C3–N1	1.45	1.45	1.45	1.46	1.45	1.45
N1–C11	1.34	1.33	1.33	1.33	1.32	1.33
C11–O3	1.23	1.23	1.24	1.24	1.24	1.23
C11–C12	1.50	1.50	1.50	1.50	1.50	1.51
C12–C13	1.37	1.37	1.39	1.38	1.37	1.37
C13–C14	1.39	1.39	1.39	1.38	1.39	1.39
C14–C15	1.38	1.38	1.40	1.39	1.39	1.39
C15–C16	1.38	1.37	1.40	1.38	1.38	1.38
C16–C17	1.39	1.39	1.39	1.39	1.38	1.39
C17–C12	1.37	1.38	1.39	1.38	1.39	1.38
C15–C18	1.49	1.50	1.48	1.49	1.50	1.50
C18–C19	1.39	1.40	1.39	1.40	1.39	1.39
C19–C20	1.39	1.38	1.38	1.38	1.39	1.38
C20–C21	1.36	1.38	1.39	1.39	1.37	1.38
C21–C22	1.36	1.37	1.38	1.37	1.37	1.37
C22–C23	1.39	1.38	1.38	1.39	1.37	1.39
C23–C18	1.38	1.39	1.39	1.40	1.40	1.39

Table S7: Comparison of lattice parameters and residual values from Le baile fit of the PXRD pattern based on two unit cells. Lattice parameters obtained from SCXRD data has been given as reference.

	SCXRD	PXRD	
		Cell 1	Cell 2
a (Å)	5.0646(2)	14.5357(12)	13.7041(10)
b (Å)	8.7483(3)	8.6153(6)	13.0856(9)
c (Å)	42.4157(15)	16.5541(12)	11.4692(8)
α (deg)	90	108.248(5)	89.337(7)
β (deg)	90	103.902(4)	99.307(5)
γ (deg)	90	80.233(5)	89.436(7)
V (Å ³)	1879.27(12)	1901.1(3)	2029.4(3)
GoF	–	3.51	3.53
R_p/wR_p	–	0.0422/0.0642	0.0416/0.0646

References

- [1] V. Petricek, M. Dusek and L. Palatinus, *Z. Kristallogr.* **229**, 345 (2014).
- [2] V. Petricek et al, JANA2020, Institute of Physics, Prague, Czech Republic (2022).
- [3] A. A. Coelho, *J. Appl Crystallogr.* **51**, 210 (2018).
- [4] A. A. Coelho, *J. Appl Crystallogr.* **36**, 86 (2003).